ARTICLE OPEN

Check for updates

Biquadratic exchange interactions in two-dimensional magnets

Alexey Kartsev [1], Mathias Augustin[1], Richard F. L. Evans [2], Kostya S. Novoselov[3,4] and Elton J. G. Santos [5 ✉]

Magnetism in recently discovered van der Waals materials has opened several avenues in the study of fundamental spin interactions in truly two-dimensions. A paramount question is what effect higher-order interactions beyond bilinear Heisenberg exchange have on the magnetic properties of few-atom thick compounds. Here we demonstrate that biquadratic exchange interactions, which is the simplest and most natural form of non-Heisenberg coupling, assume a key role in the magnetic properties of layered magnets. Using a combination of nonperturbative analytical techniques, non-collinear first-principles methods and classical Monte Carlo calculations that incorporate higher-order exchange, we show that several quantities including magnetic anisotropies, spin-wave gaps and topological spin-excitations are intrinsically renormalized leading to further thermal stability of the layers. We develop a spin Hamiltonian that also contains antisymmetric exchanges (e.g., Dzyaloshinskii–Moriya interactions) to successfully rationalize numerous observations, such as the non-Ising character of several compounds despite a strong magnetic anisotropy, peculiarities of the magnon spectrum of 2D magnets, and the discrepancy between measured and calculated Curie temperatures. Our results provide a theoretical framework for the exploration of different physical phenomena in 2D magnets where biquadratic exchange interactions have an important contribution.

INTRODUCTION

The finding of magnetism in atomically thin van der Waals (vdW) materials[1,2] has attracted an increasing amount of interest in the investigation of magnetic phenomena at the nanoscale[3]. Important in the understanding and applications of 2D vdW magnets in real technologies is the elucidation of fundamental interactions that determine their magnetic properties, such as the exchange interactions between the spins. These interactions govern the magnetic ordering and can be either symmetric, which determine collinear ferromagnets and anti-ferromagnets, or antisymmetric, which promote topological non-trivial spin textures, e.g. skyrmions. Higher-order exchange terms involving the hopping of two or more electrons play a pivotal role in the spin-ordering of low-dimensional nanostructures. For instance, biquadratic (BQ) exchange interactions are critical in the elucidation of the magnetic features of several systems, such as multilayer materials[4], perovskites[5], iron-based superconductors[6,7], iron tellurides[8] and oxides[9]. Indeed, in materials where the exchange is for some reason weak[10] (e.g., low-temperature magnets) BQ exchange has a particularly strong influence being the case of several 2D magnets discovered so far[11,12].

Here we identify that several families of 2D magnets including metals, insulators and small band gap semiconductors, develop substantially large BQ exchange interactions. The delicate interplay between the superexchange process through the non-magnetic atom and the Coulomb repulsion at neighboring spin-sites involving more than one electron induces sizable corrections to the total energy of the systems beyond bilinear spin models, e.g., Kitaev, Heisenberg, Ising. We developed a generalized non-Heisenberg spin Hamiltonian that includes both BQ and Dzyaloshinskii-Moriya interactions (DMI), providing a universal picture of the spin properties of 2D vdW magnets. We show that while BQ exchange interactions give substantial contributions to the thermal properties,

such as in critical temperatures (T_c), non-collinear spin effects via DMI are negligible. The model also offers insights via analytical equations into the spin excitations of 2D materials as a general formalism is developed for materials that hold honeycomb crystal structure, ferromagnetism and out-of-plane easy axis in a universal basis. Our results provide the conceptual framework to understand a variety of 2D magnetic materials in a consistent way explaining numerous experimental observations, including controversies on the magnetic properties of CrI_3 or $CrBr_3$.

RESULTS

Biquadratic exchange interactions

In order to calculate the different exchange contributions to the total energy at the level of first-principles methods (see Supplementary Sections 1–4 for details), we map the angular dependence of the spins $\mathbf{S}_j = \mu_s \mathbf{s}_j$, where μ_s is the magnetic moment and $|\mathbf{s}_j| = 1$, in the unit cell of the layered material[5,13,14] (Fig. 1a). We rotate the spins by θ between two known spin configurations: from ferromagnetic (FM) at $\theta = 0$, to anti-ferromagnetic (AFM) at $\theta = 180°$. Small steps in θ generate a path of quasi-continuously configurations where both energy and magnetization are allowed to relax self-consistently without any fixed constraint on the direction. The resulting curve in energy includes contributions from bilinear (BL) exchanges up to higher-order terms, e.g., BQ exchange interactions. We used different supercells that resulted in no variations of the results. We quantify the contribution of each kind of interactions using the following non-Heisenberg spin Hamiltonian:

$$\mathcal{H} = -\sum_{ij} J_{ij}(\mathbf{S}_i \cdot \mathbf{S}_j) - \sum_{ij} \lambda_{ij} S_i^z S_j^z - \sum_i D_i(\mathbf{S}_i \cdot \mathbf{e}_i)^2 - \sum_{ij} K_{ij}(\mathbf{S}_i \cdot \mathbf{S}_j)^2$$

$$(1)$$

[1]School of Mathematics and Physics, Queen's University, Belfast BT7 1NN, UK. [2]Department of Physics, The University of York, York YO10 5DD, UK. [3]Department of Material Science & Engineering, National University of Singapore, Block EA, 9 Engineering Drive 1, Singapore 117575, Singapore. [4]Chongqing 2D Materials Institute, Liangjiang New Area, Chongqing 400714, China. [5]Institute for Condensed Matter Physics and Complex Systems, School of Physics and Astronomy, The University of Edinburgh, Edinburgh EH9 3FD, UK. ✉email: esantos@ed.ac.uk
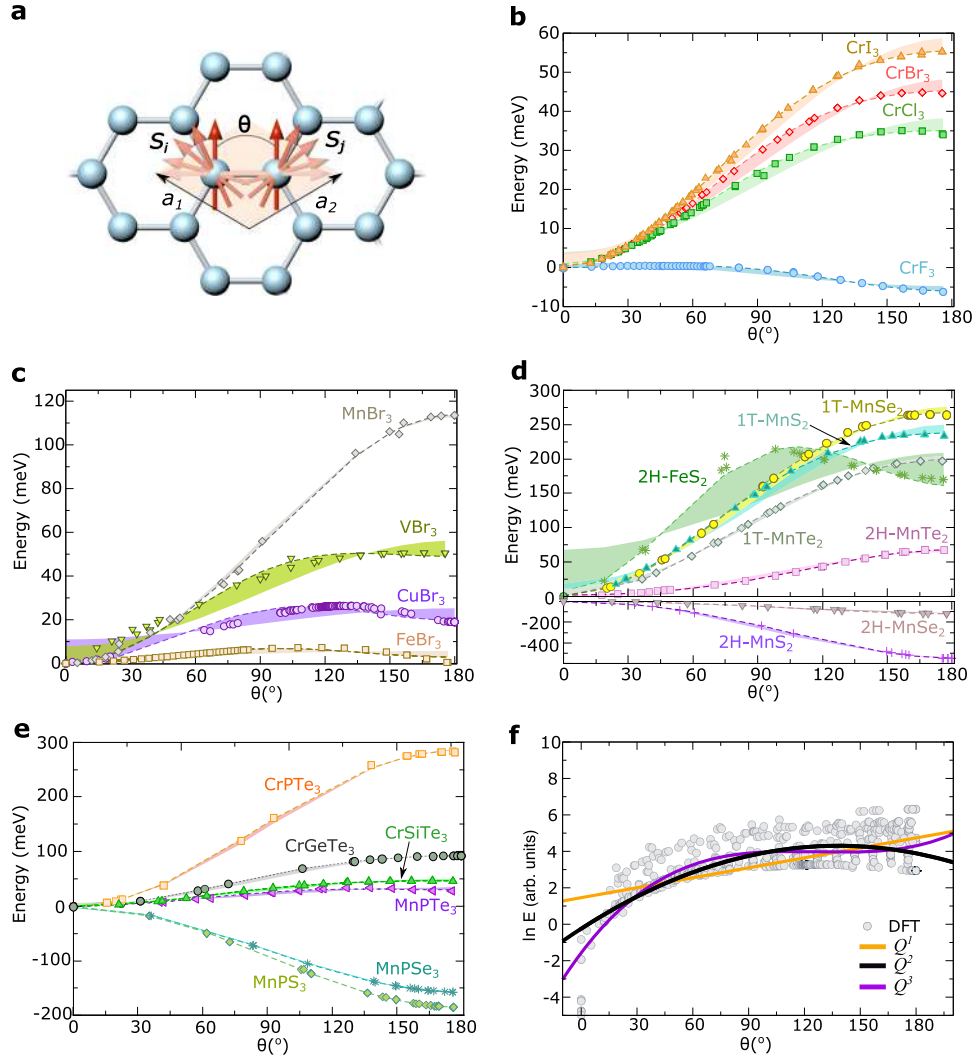
Fig. 1 Biquadratic exchange interactions in 2D magnets. a Diagram of the rotation of spins S_i and S_j in the unit cell (defined by vectors $\mathbf{a}_1$ and $\mathbf{a}_2$) of a 2D magnet by a relative angle θ between them. Spins are rotated symmetrically in opposite directions from 0° to 180°. **b–e** Relative total energy (eV) as a function of θ(°) for different monolayers of 2D magnets: trihalides (CrX$_3$, X = F, Cl, Br, I), metal tribromides (MBr$_3$, M = Mn, Cu, Fe, V), chromium based ternary tellurides (Cr$_2$X$_2$Te$_6$, X = Ge, P, Si), manganese based ternary chalcogenides (Mn$_2$P$_2$X$_6$, X = S, Se, Te), transition metal dichalcogenides (MnX$_2$, X = S, Se, Te) of different phases (2H, 1T) and an iron-based dichalcogenide (2H-FeS$_2$). The reference energy is taken at 0° as the spins oriented at the same direction. Rotations can occur in-plane or out-of-plane with similar behavior. Symbols are calculated energies. Dashed lines correspond to a quadratic fitting using $E_{bq}^{tot}(\theta) = A_0^{bq} + A_1^{bq} \cdot S^2 \cos(\theta) + A_2^{bq} \cdot S^4 \cos^2(\theta)$, while color filling areas indicate the deviation between the quadratic E_{bq}^{tot} and a linear fitting using $E_{bl}^{tot}(\theta) = A_0^{bl} + A_1^{bl} \cdot S^2 \cos(\theta)$. Materials that show large deviation, such as CuBr$_3$ or 2H-FeS$_2$, develop large BQ exchange interactions. **f** Logarithm of the total energies (DFT) for the dataset in **b–e**, as a function of θ. Data analytics using polynomial regression (least-squares algorithm) in terms of linear (Q^1), quadratic (Q^2) and cubic (Q^3) approaches is evaluated over the calculated DFT energies (dots).

where J_{ij} and λ_{ij} are the isotropic and anisotropic BL exchanges between spins $\mathbf{S}_i$ and $\mathbf{S}_j$ on atomic sites i and j; D_i is the on-site anisotropy with easy axis $\mathbf{e}_i$; and K_{ij} is the BQ exchange interactions which is due to electron hopping between two adjacent sites[15]. We restrict the discussions to first nearest-neighbor BQ interactions, that is, $K_{ij} = K_{bq}$, and $K_{ij} = 0$ otherwise. This assumption has been shown to be sufficient to study a variety of magnetic systems with higher-order exchanges[5,6,8,9]. We can write Eq.(1) in a similar form separating the terms with angular and non-angular dependence as $E_{bq}^{tot}(\theta) = A_0^{bq} + A_1^{bq} \cdot S^2 \cos(\theta) + A_2^{bq} \cdot S^4 \cos^2(\theta)$, where S is the spin moment. The different coefficients can be interpreted as the corresponding amount of BL (A_1^{bq}) and BQ (A_2^{bq}) exchanges, and the on-site energy as the spins are perpendicular to each other (A_0^{bq}). Supplementary Section 4 gives a thorough discussion on these coefficients and how to extract analytical equations for their interpretation using

Eq. (1). We extract A_0^{bq}, A_1^{bq} and A_2^{bq} from first-principles simulations for the variation of the total energy versus θ (Supplementary Section 5).

We apply this procedure for a total of 50 compounds including the most common 2D magnets studied up to date including several families of trihalides (MX$_3$, M = Ti, V, Cr, Mn, Fe, Ni, Cu; X = F, Cl, Br, I), metal tribromides (MBr$_3$, M = Mn, Cu, Fe, V), chromium based ternary tellurides (Cr$_2$X$_2$Te$_6$, X = Ge, P, Si), metal based ternary chalcogenides (M$_2$P$_2$X$_6$, M=V, Cr, Mn, Fe, Co, Ni; X = S, Se, Te), and transition metal dichalcogenides (MX$_2$, M = Co, Fe, V; X = S, Se, Te) of different phases (2H, 1T). Surprisingly, as the spins are spatially rotated away a sizable deviation from a $\cos\theta$-like behavior characteristic of BL exchange interactions (shaded area) is observed (Fig. 1b–e). The overall trend seems independent of the stoichiometric formula or the atomic elements composing the structure. The universal character of the higher-order exchange

Table 1. Calculated biquadratic exchange (K_{bq}) for several 2D magnetic materials with honeycomb (faint blue) and hexagonal (faint red) lattices using non-collinear ab initio methods as explained in the text.

Material	μ_M (μ_B)	S	K_{bq} (meV)
CrI$_3$	3.36	1.5	0.21
CrBr$_3$	3.17	1.5	0.22
CrCl$_3$	3.05	1.5	0.21
CrF$_3$	2.94	1.5	0.09
MnBr$_3$	3.88	2	0.04
CuBr$_3$	0.53	1	39.16
FeBr$_3$	3.88	2	0.06
VBr$_3$	1.93	1	2.85
CrGeTe$_3$	2.81	1.5	0.35
CrPTe$_3$	2.92	1.5	0.35
CrSiTe$_3$	3.13	1.5	0.31
MnPS$_3$	4.24	2	0.02
MnPSe$_3$	4.21	2	0.02
MnPTe$_3$	3.93	2	0.11
1T-MnSe$_2$	3.49	1.5	0.74
2H-MnSe$_2$	3.49	2	0.15
1T-MnTe$_2$	3.71	2	0.14
2H-MnTe$_2$	3.78	2	0.10
1T-MnS$_2$	3.28	1.5	1.09
2H-MnS$_2$	3.27	1.5	1.55
2H-FeS$_2$	2.18	1	20.11

The magnitudes of the spin angular momentum (S) used in the model (Supplementary Section 4) and the magnetic moments at the metal atoms (μ_M) are also included.

process in layered materials can be appreciated clearer in Fig. 1f where data-analytics using regression algorithms (linear, quadratic, cubic) was evaluated over the computed data. The best match between regression and DFT energies is for regressions beyond linear. This suggested that even more complex magnetic interactions may take place in 2D magnetic materials such as 3-, 4-spin interactions[16,17], and chiral biquadratic[18,19] which are not studied here. Materials with alike chemical environment (e.g., bond lengths, electron affinity, binding energy) such as CrI$_3$, CrBr$_3$ and CrCl$_3$ present close variation of the energy and consequently similar magnitudes of the BQ exchange (Table 1). Other compounds tend to gain energy with the spin rotation and stabilize in a different magnetic coupling, for instance, CrF$_3$ (Fig. 1b) becomes AFM ordered. This is also the case of Mn-based compounds, 2H-MnS$_2$, 2H-MnSe$_2$, MnPS$_3$, MnPSe$_3$ (Fig. 1d, e), which agreed with magnetometry measurements[20–22]. It is noteworthy that CuBr$_3$ and 2H-FeS$_2$ have substantially larger magnitudes of BQ exchange (Table 1) comparable to more complex materials, i.e., ferropnictides, where spin and electronic correlations are known to play a key role in the determination of their superconducting and strongly-correlated properties[23]. Both CuBr$_3$ and 2H-FeS$_2$ have relatively small BL exchange in the range of $5.87-6.88$ meV with $S = 1$. For materials with small BL exchange higher-order exchange tends to be sizeable[10]. This result calls for further theoretical and experimental work on these two compounds whether unusual electronic interactions can be found. Furthermore, we noticed that several other compounds could not show a clear trend with θ apart from those where a specific magnetic ordering is stabilized, e.g., $\theta = 0$, 180° (Supplementary Section 6). Materials that are unable to stabilize different spin

orientations are either due to strong magnetic anisotropy where a preferential spin orientation is too strong to be tilted (e.g. Ising magnets) or different spin solutions are not energetically stable ending up in non-magnetic phases[24].

We have also checked whether other models can give a sound description of the magnetic properties of the quadratic dependence of the energy as a function of θ. In particular, we considered two models: a Kitaev model[25,26], and a Heisenberg model including biquadratic on-site magnetic anisotropy. For the latter, the magnitudes of the biquadratic on-site anisotropies are several orders of magnitude smaller than BQ exchange within the range $3.87-14.32\mu eV$ (see details in Supplementary Section 7). For the former, there is no quadratic dependence on θ for the Kitaev model. We can expand the Kitaev Hamiltonian[25] assuming a rotation by angle θ between the spins to show that a fitting equation of the form of $E_{Kitaev}^{tot}(\theta) = B_0 + B_1 \sin(2\theta)$ can be extracted (see details in Supplementary Section 8). These results suggest that BL models are insufficient to describe the magnetic features of 2D vdW magnets.

A Hubbard-based microscopic model

To understand the microscopic mechanism of the BQ exchange in 2D materials, we will use the following 2D half-filled Hubbard Hamiltonian applied to the honeycomb lattice (Fig. 2a, b):

$$H = -t_{eff} \sum_{\langle ij \rangle, \sigma} c_{i,\sigma}^\dagger c_{j,\sigma} + U \sum_i n_{i\uparrow} n_{i\downarrow} + \sum_{i,\sigma} \mu_{i,\sigma} n_{i,\sigma}, \quad (2)$$

where indices i and j denote the lattice sites, the d-spin states on the metal atoms (M$_{A,B}$) are labeled as $\sigma = \uparrow, \downarrow$, the sum $<ij>$ is over the nearest neighbors and t_{eff} is the effective nearest neighbor hoping between M$_{A,B}$ ions. t_{eff} is due to the hybridization between $3d^n$ and np orbitals ($n = 2, 3, 4, 5$ depending on the atomic element involved) at M$_{A,B}$ and X atoms, respectively (Fig. 2b). The direct hopping between M$_{A,B}$ scales with $t_{dd} \sim r^{-5}$ and therefore for relatively big distances can be neglected[15]. $U > 0$ is the non-negative on-site Coulomb repulsion, $c_{i,\sigma}^\dagger(c_{i,\sigma})$ is the creation (annihilation) operator for a fermion with spin σ at site i, $n = c_{i,\sigma}^\dagger c_{i,\sigma}$ is the density operator and $\mu_{i,\sigma}$ is the chemical potential which controls the filling of the bands. Second-order perturbation theory in Eq.(2), assuming $U >> t_{eff}$, gives the energy contributions of the Heisenberg exchanges[27,28]:

$$\begin{aligned} J_{FM}^{(2)} &= t_{eff}^2/(U - U_{ex}) \\ J_{AFM}^{(2)} &= t_{eff}^2/(U + U_{ex}) \\ J_{bl} &= t_{eff}^2 \frac{2U_{ex}}{U^2 - U_{ex}^2} \end{aligned} \quad (3)$$

where $J_{FM}^{(2)}$ and $J_{AFM}^{(2)}$ are the exchange energies for FM and AFM coupling at second-order, and the BL exchange is defined as $J_{bl} = J_{FM}^{(2)} - J_{AFM}^{(2)}$. U_{ex} is an energy correction for the internal spin exchange whether a spin flip is required during the hopping between M$_{A,B}$ sites (Fig. 2b)[28]. Such term can be used to stabilize or destabilize spin transfer through the M$_{A,B}$ − X covalent bonds as the exchange occurs[15,28]. If the electron-hopping is to an occupied orbital of the neighboring site, U_{ex} will favor AFM alignment of the two spins via a superexchange interaction (see Supplementary Section 9 for details). However, if the electron-hopping is to an unoccupied or a virtual state, a FM alignment will be favored by U_{ex}[29]. The competition between the amount of energy U_{ex} to stabilize a specific coupling and the Coulomb repulsion U between the electrons at an energy state may compensate each other leading to a small value of J_{bl}. Indeed, several 2D magnets have shown low-temperature magnetism[1,2,12] which is directly related with the small magnitude of the exchange interactions. In this case, it is necessary to extend the perturbation in t_{eff}/U to fourth-order in Eq. (2) involving at least one electron
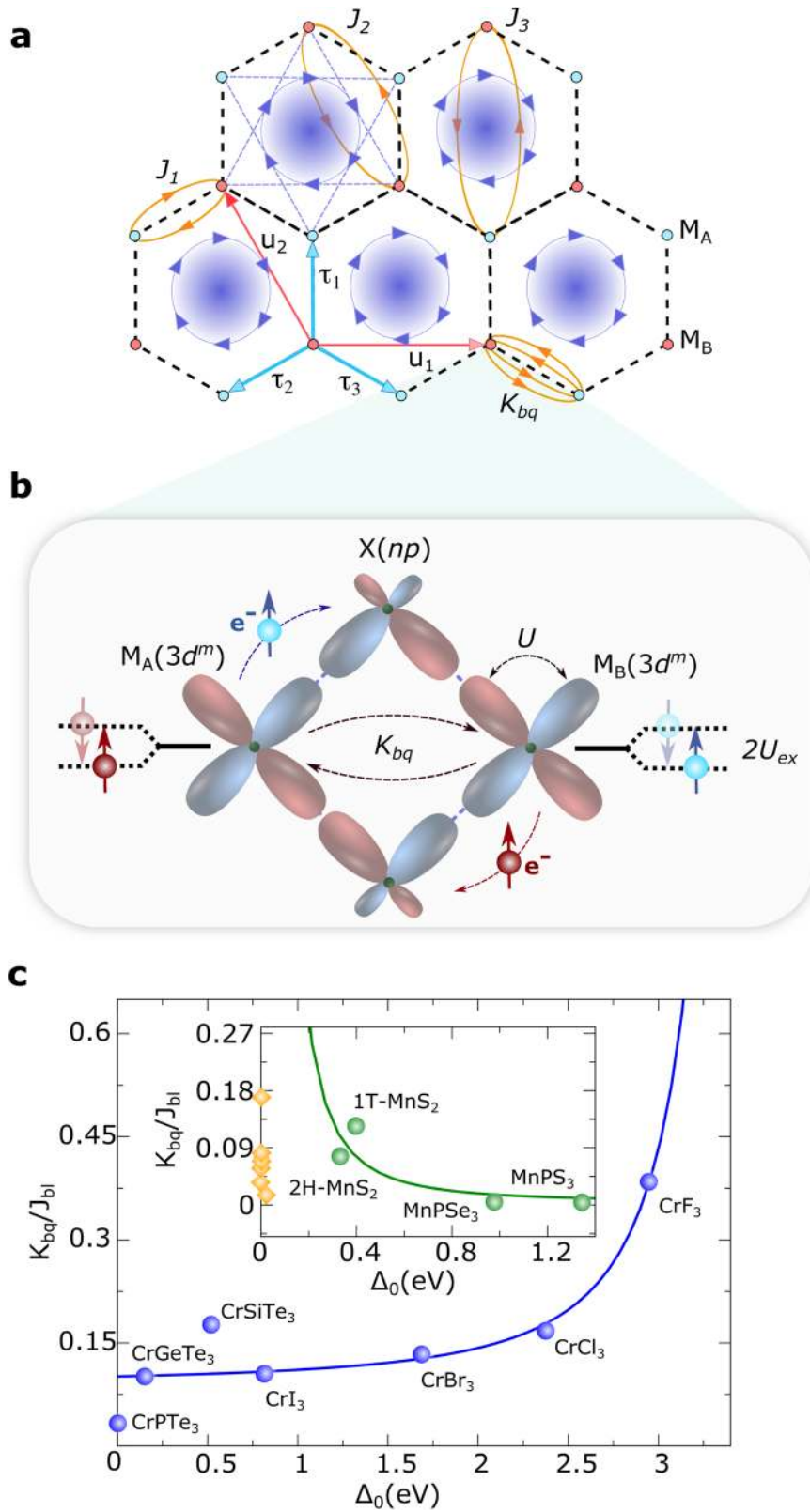
Fig. 2 Bilinear (BL) and biquadratic (BQ) exchange interactions in 2D magnets. a Schematic of the BL exchanges at first (J_1), second (J_2) and third (J_3) nearest neighbors (NN), and BQ exchange (K_{bq}) at first NN. Single and double line diagrams represent BL and BQ exchanges, respectively. The two inequivalent magnetic sites in the honeycomb lattice are shown by faint blue (M_A) and faint red (M_B) dots. The blue orbits inside of the hexagons represent the magnetic flux ϕ generated by the second-NN Dzyaloshinskii-Moriya interactions (DMI), which breaks the inversion symmetry of the lattice. The dashed lines show the magnon hopping between second NN as the magnons gain a phase given by ϕ (see text). The lattice vectors $\mathbf{u}_i$ ($i = 1, 2$) and τ_j ($i = 1, 2, 3$) show the first and second NN on the lattice, respectively. **b** Zoom-in on the BQ exchange process involving two electrons between sites M_A and M_B with $3d^m$ electrons in the valence. The BQ exchange K_{bq} is mediated by non-magnetic atoms X with a valence given by np electrons, where n will depend on the atomic elements involved. An on-site Hubbard U term is at the $M_{A,B}$ sites with U_{ex} representing the potential spin-splitting when the spins of the electrons involved in the BQ exchange align ferro- or anti-ferromagnetically (Supplementary Section 4). The difference between up and down spin coupling is given by $2U_{ex}$. **c** K_{bq}/J_{bl} versus Δ_0(eV) for all materials displaying BQ exchange interactions. Magnetic atoms with similar chemical environment in terms of Coulomb repulsion, exchange interactions and valence follow alike behavior for K_{bq}/J_{bl}. For instance, Cr in blue and Mn in green (inset). Orange dots show materials with dissimilar electronic configurations but with $\Delta_0 = 0$.

from both $M_{A,B}$ sites which resulted in[15]:

$$
\begin{aligned}
J_{FM}^{(4)} &\propto t_{eff}^4/(U - U_{ex})^3 \\
J_{AFM}^{(4)} &\propto t_{eff}^4/(U + U_{ex})^3 \\
K_{bq} &= t_{eff}^4 \frac{2(3U^2 U_{ex} + U_{ex}^3)}{(U^2 - U_{ex}^2)^3}
\end{aligned}
\tag{4}
$$

with $K_{bq} = J_{FM}^{(4)} - J_{AFM}^{(4)}$ being the BQ exchange energy. Both Eqs. (3)–(4) show that a competition between FM and AFM couplings takes place once the electrons are hopping between different spin sites. The stabilization of one or another magnetic order is determined by several factors such as the ligand-field splitting Δ_0 between t_{2g} and e_g states in the metal atom in the honeycomb lattice. As the filling of both type of states determines the magnitude of the $3d - sp$ hybridization between metals and ligands, we can approach $\Delta_0 \approx U - U_{ex}$ being proportional to the bandgap of the material[10]. This condition is valid as long as the magnitudes of U and U_{ex} do not compete to each other. Since U_{ex} is an energy correction of spin stabilization, it should comply with Hund's rule where unpaired spins occupy other states of the $3d$ shell (Fig. 2b). It has been shown that the role of high-order exchange interactions increases on reduction of the bandgap mediated by the non-magnetic atoms which is related to the ratio of BQ and BL exchanges[27,30]. If we divide Eq. (4) and Eq. (3) and use the definition of Δ_0, we can write a direct relationship between the exchange interactions and the bandgap for 2D magnets as:

$$
K_{bq}/J_{bl} = t_{eff} \frac{4U^2 + \Delta_0^2 - 2U\Delta_0}{\Delta_0^2 (2U - \Delta_0)^2}
\tag{5}
$$

This equation can be understood as a direct interplay between the Coulomb repulsion and the hopping of electrons between different sites subjected to the crystal field or bandgap of the material. We can consider two situations in Eq. (5): $\Delta_0 \to 0$ and $\Delta_0 \to 2U$ which correspond to small and large bandgap materials, respectively. This resulted in:

$$
K_{bq}/J_{bl} \propto t_{eff} \frac{1}{(\Delta_0)^2}\bigg|_{\Delta_0 \to 0}
\tag{6}
$$

$$
K_{bq}/J_{bl} \propto t_{eff} \frac{1}{(2U - \Delta_0)^2}\bigg|_{\Delta_0 \to 2U}
\tag{7}
$$

Fig. 2c shows the variation of K_{bq}/J_{bl} as a function of Δ_0 for the core of materials displaying BQ exchange interactions. Strikingly, both Eqs. (6)–(7) correctly describes the overall behavior observed in our simulations. Materials with similar bonding environment, for instance, either in terms of Cr (Mn) atoms follow an increase (decrease) of K_{bq}/J_{bl} with the bandgap, respectively. It is worth mentioning that as the compounds tend to a AFM spin alignment[10,29], i.e., CrF_3, they increase the value of K_{bq}/J_{bl} being the case within the Cr-based trihalide family (CrX_3, X = F, Cl, Br, I). There is also an abrupt change in behavior for narrow bandgap materials and metals with no dependence on Δ_0 (inset in Fig. 2c).

These results indicate that one can design the amount of BQ exchange in a 2D magnet tuning its bandgap, for instance using an electric bias as recently used in CrI_3[31].

Thermal effects in 2D magnets

To verify whether BQ exchange interactions will have any effect on the thermal properties of 2D vdW magnets, we have implemented Eq. (1) within the Monte Carlo Metropolis algorithm with an adaptive move[32]. In the spin model we assume a classical spin vector $\mathbf{S}_i$ on each atomic site i. The quantization vector for the spin is a local quantity which intrinsically includes the effects of local thermal spin fluctuations, magnon processes and spin excitations. In our implementation the BQ exchange is quite general and can be applied to any pair-wise exchange interaction of arbitrary range. We also consider an additional term in Eq. (1) including the local Zeeman field $\mathbf{B}$ on the magnetic ions with a length of the local atomic moment μ_i arising from the BQ exchange interactions as:

$$
\begin{aligned}
\mathcal{H} = &-\sum_{ij} J_{ij}(\mathbf{S}_i \cdot \mathbf{S}_j) - \sum_{ij} \lambda_{ij} S_i^z S_j^z - \sum_i D_i(\mathbf{S}_i \cdot \mathbf{e}_i)^2 \\
&- \sum_{ij} K_{ij}(\mathbf{S}_i \cdot \mathbf{S}_j)^2 - \sum_i \mu_i \mathbf{S}_i \cdot \mathbf{B}_i
\end{aligned}
\tag{8}
$$

For atomistic spin dynamics simulations, the effective field due to the biquadratic exchange are calculated via the first-derivative of Eq. (8) on the different spin components as:

$$
H_{bq,i}^l = -\frac{1}{\mu_i} \frac{\partial \mathcal{H}}{\partial S_i^l} = 2K_{bq} S_j^l (\mathbf{S}_i \cdot \mathbf{S}_j)
\tag{9}
$$

where $l = x, y, z$ represents the geometrical coordinates at the atomic sites $i(j)$, and $(\mathbf{S}_i \cdot \mathbf{S}_j) = S_i^x S_j^x + S_i^y S_j^y + S_i^z S_j^z$. The effective field $H_{bq,i}^l$ therefore contributes to the total field describing the time evolution of each atomic spin using the stochastic Landau-Lifshitz-Gilbert equation[33]. We calculate up to third nearest-neighbors λ_{ij} and J_{ij} in Eq. (1) on a representative set of 2D magnets, e.g., Cr-based trihalide family (Table 2). Supplementary Section 10 gives a thorough discussion on the calculation of the exchange parameters. Figure 3 shows the behavior of the magnetization (M/M_0, where M_0 is the saturation magnetization at 0 K) and the logarithm of the magnetic susceptibility ($\ln \chi$) as a function of temperature T(K) for CrI_3, $CrBr_3$ and $CrCl_3$. Intriguingly, the inclusion of BQ exchange interactions give sizable thermal effects on both M/M_0 and $\ln \chi$ for all materials (Supplementary Section 11). By fitting the Monte Carlo simulations with $M(T) = M_0\left(1 - \frac{T}{T_c}\right)^\beta$ (where β is the critical exponent) we can notice that the Curie temperatures T_c changes by several Kelvins with the inclusion of BQ exchange interactions. The calculated magnitudes of T_c for CrI_3 and $CrBr_3$ approach closely those measured for both compounds with almost no difference (Fig. 3a–d). The lack of experimentally measured T_c for monolayer $CrCl_3$ unable us to make a clear comparison with our simulations. The different amount of

Table 2. Computed values of several magnetic quantities for CrX$_3$ (X = I, Br, Cl, F) at different number of nearest neighbors: isotropic (J_1, J_2, J_3) and anisotropic (λ_1, λ_2, λ_3) BL exchanges.

Comp.	J_1 (meV)	J_2 (μeV)	J_3 (μeV)	λ_1 (μeV)	λ_2 (μeV)	λ_3 (μeV)	D (μeV)
CrI$_3$	2.01	320.02	8.10	106.8	−10.24	0.91	108.82
CrBr$_3$	1.66	164.35	−11.60	20.69	−2.06	−0.69	34.09
CrCl$_3$	1.28	72.03	−25.18	20.07	−9.74	−0.51	12.67
CrF$_3$	−0.23	17.27	0.20	3.33	−0.67	−0.14	122.02

The on-site magnetic anisotropy D is also included. See Supplementary Section 4 for details.
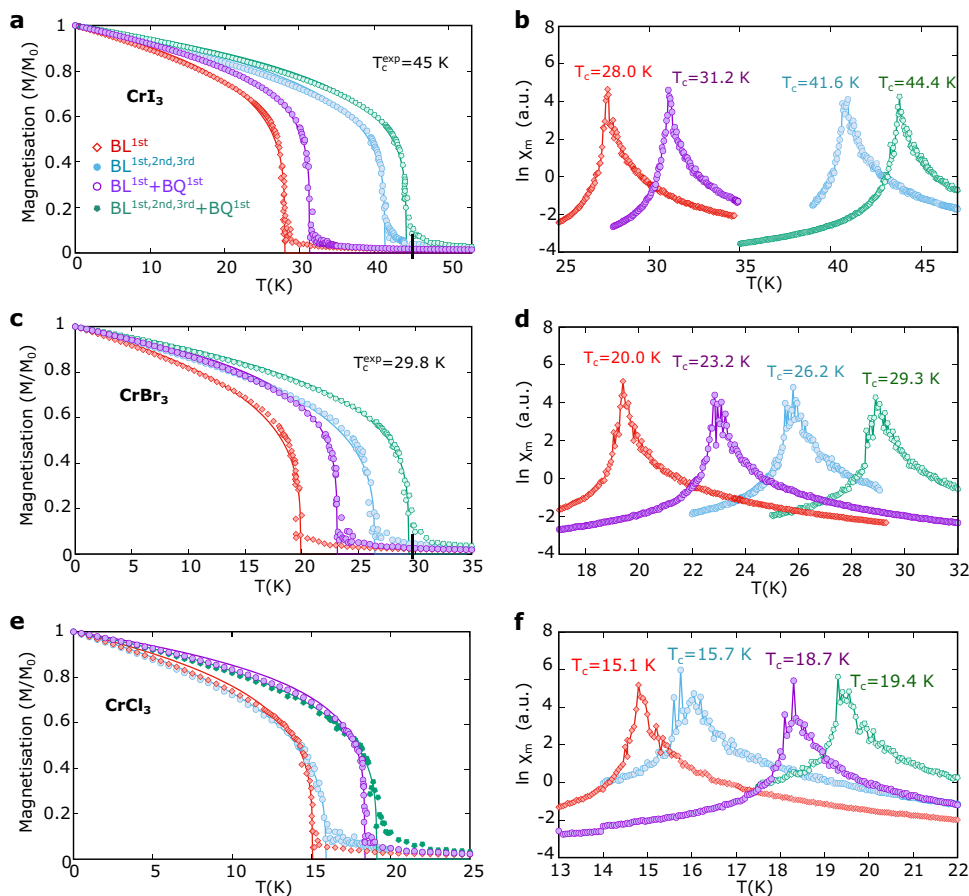
Fig. 3 Monte-Carlo simulations at different levels of theory including BL and BQ exchange interactions. a, b Magnetization (M/M_0) and logarithm of the magnetic longitudinal susceptibility lnχ_m (a.u.) versus temperature (K), respectively, for monolayer CrI$_3$. Calculated and fitting curves using $M/M_0 = (1 - T/T_c)^\beta$ (where T_c and β are the critical temperature and coefficient, respectively) are shown by dots and solid lines, respectively, in **a**. Solid lines in **b** show the interpolation between points. Different curves correspond to different number of NN, from one up to third, taken into account in BL interactions: BL^{1st} (faint red), BL^{1st,2nd,3rd} (faint blue). Results including BQ exchange at first NN (BQ^{1st}) with different number of BL exchanges are shown in purple (BL^{1st} + BQ^{1st}) and faint green (BL^{1st,2nd,3rd} + BQ^{1st}). Critical temperatures (T_c) at each level of BL and BQ exchange interactions are indicated at **b** with the maximum magnitude of lnχ_m (a.u.) highlighted. Magnetic susceptibility is shown in logarithm scale for clarify. Experimental critical temperature (T_c^{exp}) is included for comparison. **c, d** and **e, f** similar plots as in **a, b**, for CrBr$_3$ and CrCl$_3$, respectively. Critical exponents β extracted from the simulations for BL^{1st,2nd,3rd} + BQ^{1st} are β = 0.22, 0.24 and 0.28 for CrI$_3$, CrBr$_3$ and CrCl$_3$ respectively. Magnitudes of β for BL^{1st,2nd,3rd} are 0.25, 0.28 and 0.32 for CrI$_3$, CrBr$_3$ and CrCl$_3$ respectively.

nearest-neighbors at BL exchanges (from 1st to 3rd) also produces substantial effects even though not enough to reproduce the experimental values of T_c for CrI$_3$ and CrBr$_3$. It is worth mentioning that different groups have reported distinct magnitudes of T_c for CrBr$_3$[34–36][,37–39], which may be due to different factors such as sample quality, defects, and doping levels. We believe that our simulations still provide an accurate picture showing the effects of the underlying exchange interactions for these low-dimensional magnets at the limit of an ideal, pristine crystal (see Supplementary

Section 12). Moreover, several other materials display larger values of BQ exchange interactions (Table 1) indicating that higher-exchange interactions should be taken into account on the description of their magnetic properties.

Enhancement of magnetic stability

An outstanding remark on the existence of BQ interactions in 2D magnets is on the implications on their magnetic features. It is

well known that several materials developed macroscopic properties due to this higher-order exchange interactions. From paramagnetic measurements of Mn^{+2} ions in MgO[9], up to different magnetic phases in oxides[5,13],40, it is not clear whether BQ exchange induces any significant role effect on basic properties, such as critical temperatures or stability. To understand the intrinsic effect of higher-order exchange interactions in the thermal features of 2D magnetic materials and provide a consistent description of the underlying spin interactions, we have developed an analytical model based on spin-wave theory[37,38]. We generalized Eq. (1) to second order contributions on the magnetic anisotropies which resulted in:

$$\mathcal{H} = -\sum_{ij} J_{ij}(\mathbf{S}_i \cdot \mathbf{S}_j) - \sum_{ij} \lambda_{ij} S_i^z S_j^z - \sum_i D_i(\mathbf{S}_i \cdot \mathbf{e}_i)^2$$
$$- \sum_{ij} K_{ij}(\mathbf{S}_i \cdot \mathbf{S}_j)^2 - \sum_i D_i^{bq}(\mathbf{S}_i \cdot \mathbf{e}_i)^4 - \sum_{ij} \lambda_{ij}^{bq} \left(S_i^z S_j^z\right)^2$$

(10)

where D_i^{bq} and λ_{ij}^{bq} are the BQ on-site anisotropy and BQ anisotropic exchange, respectively. We replace the spin operators $\mathbf{S}_{i,j}$ in Eq. (10) by bosonic creation ($a_i^\dagger$, $b_i^\dagger$) and annihilation (a_i, b_i) operators over the honeycomb sub-lattices $\mathcal{A}$ and $\mathcal{B}$ using Holstein-Primakoff transformations[38]:

For $i \in \mathcal{A}$ sublattice:

$$S_i^z = (S - a_i^\dagger a_i)$$
$$S_i^+ \approx \sqrt{2S} a_i$$
$$S_i^- \approx a_i^\dagger \sqrt{2S}$$

For $i \in \mathcal{B}$ sublattice:

$$S_i^z = (S - b_i^\dagger b_i)$$
$$S_i^+ \approx \sqrt{2S} b_i$$
$$S_i^- \approx b_i^\dagger \sqrt{2S}$$

where we assume that $a_i^\dagger a_i \ll S$ and $b_i^\dagger b_i \ll S$ for small deviations of the spins from their ground state orientations. This gives (see Supplementary Section 13 for details):

$$\tilde{\mathcal{H}} = \sum_i \left(2\tilde{D}S + Z \cdot S(\tilde{J} + \tilde{\lambda})\right)(b_i^\dagger b_i + a_i^\dagger a_i) - \tilde{J}S \sum_{\langle ij \rangle} \left(a_i^\dagger b_j + b_j^\dagger a_i\right)$$

(11)

where the sum over i and j runs over the sub-lattices and first nearest neighbors, respectively, and Z is the number of first nearest-neighbors. This procedure outlines a strong implication of the inclusion of higher-order exchange interactions in the description of the magnetic properties of 2D magnets. That is, the enhancement of several magnetic quantities:

$$\tilde{J} \approx J + 2S^2 \cdot K_{bq}$$

(12)

$$\tilde{\lambda} \approx \lambda + 2S^2 \cdot \lambda^{bq}$$

(13)

$$\tilde{D} \approx D + 2S^2 \cdot D^{bq}$$

(14)

where λ^{bq} and D^{bq} are the BQ anisotropic exchanges, and the BQ on-site magnetic anisotropy, respectively, for first nearest neighbors. Incidentally Eqs. (12)–(14) yield several implications on the magnetic properties of the sheets, in particular, on the stabilization of magnetism in truly 2D. It is well known that in order to overcome thermal fluctuations that could destroy any magnetic order[39], sizable magnetic anisotropies need to be developed to gap the low-energy modes in the magnon spectra. That is, a spin wave gap needs to appear at the energy dispersion to act as a barrier to excitations of long-wavelength spin waves. We can show that the relation between the spin wave gap taken into account BQ exchange interactions (Δ_{bq}) and that at the level BL exchange (Δ_{bl}) for first-nearest neighbors is given by (see Supplementary Section 13):

$$\Delta_{bq} = \Delta_{bl} + 4S^3(D^{bq} + \frac{3}{2}\lambda^{bq})$$

(15)

where $\Delta_{bl} = 2S[D + \frac{Z\lambda}{2}]$. By using some parameters for monolayer CrI_3 from Table 2, and approaching the second term in Eq. (15) as $D^{bq} + 3\lambda^{bq} \approx 10.72\,\mu eV$ (see Supplementary Section 7) we can estimate $\Delta_{bl} = 0.81$ meV and $\Delta_{bq} = 1.0$ meV. The magnitude of Δ_{bq} is consistent with recent measurements of the magnon dispersion for bulk CrI_3, which a spin wave gap of approximately 1.3 meV was measured[40]. Furthermore, the increment of the on-site and anisotropic magnetic anisotropies (Eqs. (13)–(14)) indicates that not only spin-orbit mechanisms are behind the substantial anisotropy in CrI_3 but rather higher-order exchange processes. Such BQ exchange-driven large magnetic anisotropy mechanism has been proposed for iron-based superconductors[7,23,41] which successfully described their magnetic properties. A direct consequence Eqs. (12)–(14) is the increment of Curie temperatures by factor r given by (see Supplementary Section 13):

$$r = \frac{\tilde{T}_C}{T_C} \approx \frac{\tilde{J}\ln\left(1 + 2\pi JS/\Delta_{bl}\right)}{J\ln\left(1 + 2\pi \tilde{J}S/\Delta_{bq}\right)}.$$

(16)

where $\tilde{T}_C$ and T_C are the Curie temperatures with and without BQ interactions, respectively. Including few values in Eq. (16), we can roughly estimate an enhancement of $r \approx 39\%$ for monolayer CrI_3 which follows the Monte Carlo calculations (Fig. 3a, b). It is worth noticing that the model in Eq. (11), i) takes into account only first-nearest neighbors in the exchange interactions, and ii) we assume a mean-field approach in the solution of the non-linear Holstein-Primakoff transformation (e.g. magnon-magnon interactions) to simplify the complex mathematical terms, i.e. four-operator product. Supplementary Section 14 provides a full discussion on the details involved.

Describing topological spin excitations through BQ and DMI

An intriguing question that raised by the presence of BQ exchange interactions is whether they play an important role in the description of magnetic quasiparticles such as magnons and non-trivial spin textures in 2D vdw magnets. It has recently been shown using neutron scattering[40] that CrI_3 magnet shows topological spin-excitations with two distinctive magnon bands separated by a bandgap of 4 meV at the Dirac $\mathbf{K}$-point. In spite of the clear demonstration that CrI_3 can not follow an Ising model as initially pointed out[1], these results indicate that non-Heisenberg interactions play an important role in the creation of spin-excitations in 2D magnetic materials. Since the gap opening at $\mathbf{K}$ is related with the inversion symmetry breaking and appearance of DMI, chirality becomes crucial in the discrimination of the magnon bound states. Moreover, it has become well established[23,42–44] that isotropic spin interactions at the level of the BL Heisenberg models do not capture all features in the energy dispersion of spin-excitations in magnetic materials. There are additional contributions through uniaxial anisotropies, next-nearest neighbor interactions and the delicate balance between them, that need to be considered. In order to account for all these quantities, we extended the model in Eq. (1) with the addition of DMI:

$$\mathcal{H}_{latt} = \mathcal{H} + \sum_{\langle\langle ij \rangle\rangle} \mathbf{A}_{ij} \cdot (\mathbf{S}_i \times \mathbf{S}_j)$$

(17)

where $\mathbf{A}_{ij}$ is the DMI between spins $\mathbf{S}_i$ and $\mathbf{S}_j$. For a honeycomb ferromagnetic layer, with an easy axis perpendicular to the surface (z-direction), there is no breaking of the inversion symmetry of the lattice at first nearest-neighbors, e.g., $\mathbf{A}_{ij}^{1st} = 0$. However, contributions from the second nearest-neighbors become non-negligible as space inversion is not present. Therefore, we consider the DMI vector as $\mathbf{A} = v_{ij}A^z\mathbf{z}$, where A_z is the magnitude of the DMI along of the easy-axis, and $v_{ij} = \pm1$ represents the hopping of spins at

second nearest-neighbors from sites i to j and vice-versa, respectively (Fig. 2a). Similarly as shown above, we can use Holstein-Primakoff transformations for $J_i > 0$ to write Eq. (17) in terms of bosonic creation and annihilation operators (see details in Supplementary Section 15):

$$\mathcal{H}_{latt} = \mathcal{H}_{BL} + \mathcal{H}_{BQ} + \mathcal{H}_{DMI} \tag{18}$$

where we separate the terms due to BL exchange ($\mathcal{H}_{BL}$), from those due to BQ ($\mathcal{H}_{BQ}$) and DMI ($\mathcal{H}_{DMI}$) which can be written as:

$$\mathcal{H}_{BL} = H_D + \sum_{i=1}^{3} H_i^{Isotropic} + \sum_{i=1}^{3} H_i^{Anisotropic} \tag{19}$$

$$H_{BQ} = -12K_{bq}S^4 - 2K_{bq}S^3 \left(\sum_{\langle ij \rangle} \left(b_j^\dagger a_i + a_i^\dagger b_j \right) - Z_1 \sum_{i \in \mathcal{A}}^{N/2} a_i^\dagger a_i - Z_1 \sum_{i \in \mathcal{B}}^{N/2} b_i^\dagger b_i \right) \tag{20}$$

$$\mathcal{H}_{DMI} = iA_zS \left(\sum_{\langle\langle ij \rangle\rangle \in \mathcal{A}}^{N/2} \left(a_i^\dagger a_j - a_j^\dagger a_i \right) + \sum_{\langle\langle ij \rangle\rangle \in \mathcal{B}}^{N/2} \left(b_i^\dagger b_j - b_j^\dagger b_i \right) \right) \tag{21}$$

where H_D is the on-site anisotropy term, and $H_i^{Isotropic}$ and $H_i^{Anisotropic}$ are respectively the isotropic and anisotropic parts of the BL exchange Hamiltonian taken into account up to third nearest-neighbors ($i = 1, 2, 3$). The sum in $\langle ij \rangle$ runs over the first nearest-neighbors at both sublattices $\mathcal{A}$ and $\mathcal{B}$ while that on $\langle\langle ij \rangle\rangle$ runs over the second nearest-neighbors specifically on either $\mathcal{A}$ or $\mathcal{B}$ lattice. We notice that the second nearest neighbors not only break the inversion symmetry of the honeycomb lattice but also generate a magnetic flux ϕ involving A_z and J_2 given by:

$$\phi = tan^{-1}(A_z/J_2) \tag{22}$$

The magnetic flux (circular arrow) can be appreciated in Fig. 2a when the magnons (dashed lines) hop between the second nearest-neighbors. This process introduces a phase $\phi_{ij} = \mu_{ij}\phi$ ($\mu_{ij} = \pm1$) in the magnons as they hop from a site i to j, and vice-versa. The different magnitudes of μ_{ij} determine whether the hopping follows the flux and consequently induces nontrivial topological properties (e.g. chirality) similarly as in the Haldane model[45,46] for fermions. The topological features of the magnon bands can be described in the k−space by using the Fourier transform of the creation ($a_k^\dagger$, $b_k^\dagger$) and annihilation (a_k, b_k) operators in Eq. (18) as:

$$\mathcal{H} = \mathcal{H}_0 + \sum_k \begin{pmatrix} a_k^\dagger & b_k^\dagger \end{pmatrix} \begin{pmatrix} h_0(\boldsymbol{k}) + h_z(\boldsymbol{k}) & h_x(\boldsymbol{k}) - ih_y(\boldsymbol{k}) \\ h_x(\boldsymbol{k}) + ih_y(\boldsymbol{k}) & h_0(\boldsymbol{k}) - h_z(\boldsymbol{k}) \end{pmatrix} \begin{pmatrix} a_k \\ b_k \end{pmatrix} \tag{23}$$

where the different terms can be written as (see Supplementary Section 15 for details):

$$\mathcal{H}_0 = -2DS - 3(J_1 + \lambda_1)S^2 - 6(J_2 + \lambda_2)S^2 - 12KS^4$$

$$h_0(\boldsymbol{k}) = \varepsilon_0 - 4\sqrt{(J_2S)^2 + (A_zS)^2}C(\boldsymbol{k})$$

$$\varepsilon_0 = 2DS + (J_1 + \lambda_1)Z_1S + 6KS^3 + 6(J_2 + \lambda_2)S + 3J_3S$$

$$h_x(\boldsymbol{k}) = -(J_1 + 2KS^2)S\sum_{j=1}^{3}\cos(\boldsymbol{k}\cdot\boldsymbol{\tau}_j) - J_3S\sum_{j=1}^{3}\cos(\boldsymbol{k}\cdot(\boldsymbol{u}_j + \boldsymbol{\tau}_j))$$

$$h_y(\boldsymbol{k}) = -(J_1 + 2KS^2)S\sum_{j=1}^{3}\sin(\boldsymbol{k}\cdot\boldsymbol{\tau}_j) - J_3S\sum_{j=1}^{3}\sin(\boldsymbol{k}\cdot(\boldsymbol{u}_j + \boldsymbol{\tau}_j))$$

$$h_z(\boldsymbol{k}) = 4\sqrt{(J_2S)^2 + (A_zS)^2}S(\boldsymbol{k}) \tag{24}$$

where $C(\boldsymbol{k}) = \cos(\phi)\sum_{j=1}^{3}\cos(\boldsymbol{k}\cdot\boldsymbol{u}_j)$ and $S(\boldsymbol{k}) = \sin(\phi)\sum_{j=1}^{3}\sin(\boldsymbol{k}\cdot\boldsymbol{u}_j)$. The vectors $\boldsymbol{\tau}_j$ and $\boldsymbol{u}_j$ are respectively between 1st and 2nd nearest neighbors (Fig. 2a).

The eigenvalues of Eq. (23) can be written in terms of the lower and upper energy bands as:

$$E^\pm = h_0(\boldsymbol{k}) \pm \sqrt{h_x(\boldsymbol{k})^2 + h_y(\boldsymbol{k})^2 + h_z(\boldsymbol{k})^2} \tag{25}$$

Note that Eqs. (24) and (25) are general for any honeycomb material with ferromagnetic order, easy-axis perpendicular to the surface and develop DMI and BQ exchange interactions. For instance, we can use them to predict the energy dispersion of the magnon bands over the first Brillouin zone (BZ) of any 2D magnet, e.g., CrI$_3$. Figure 4a–e shows different levels of theory either using a simple XXZ model or including more sophisticated terms through the BQ exchange, DMI or simultaneously all of them. It is clear that XXZ models without any contribution from DMI (Fig. 4a–c) does not describe the gap opening at the Dirac points due to the breaking of the inversion symmetry. Moreover, a model at the level of XXZ + DMI as initially used to understand the magnon dispersion of CrI$_3$[40] does not capture entirely the full profile of the bands (Fig. 4d). The upper branch E^+ becomes nearly flat with the increment of J_2 at the path $K - M - K$ while the lower magnon branch E^- turns more curved. This picture modifies substantially when BQ exchange interactions are included in the XXZ + BQ + DMI model (Fig. 4e) as the magnon bands follow a similar curvature throughout the variation of J_2, although the upper branch at Γ increased to $E_\Gamma^+ = 27.8$ meV. A sound comparison between the XXZ + BQ + DMI model and the experimental results for CrI$_3$ is obtained (Fig. 4f) when J_1 is varied similarly (Fig. 4a) indicating that the first nearest-neighbors are important on the stabilization of E_Γ^+. It is worth mentioning that the value of the exchange interactions taken into account in the fitting of the neutron scattering spectra[40] do not separate BL contributions from BQ as shown in Eqs. (12)–(14). Hence, it is not known from the fitting procedure[40] what is the contribution of K_{bq} to the magnon dispersion. However, such separation can be clearly stated in our model as indicated in Fig. 4f. Furthermore, even though DMI is important for the gap opening at the Dirac point, it does not contribute to the magnitudes of the magnetization or critical temperatures for any 2D magnet with an out-of-plane easy-axis and ferromagnetic aligned spins (see details in Supplementary Section 15).

DISCUSSION
In summary, we have shown the importance of biquadratic exchange interaction in the magnetic properties of 2D materials. We have described the phenomenology of such higher-order spin coupling, discussed its implications on several magnetic properties, and presented results at the level of non-collinear first-principles methods, Monte Carlo approximations and analytical models. The developed spin Hamiltonian including BQ exchange and DMI provided an accurate picture of topological spin-excitations on a generalized basis for any 2D magnet. Our results are particularly timely given the increasing interest in quantum materials, and we believe that our work will motivate the exploration of different exchange couplings and competition between critical phenomena[47].

The effects of the BQ exchange interactions proposed here should manifest in experimentally accessible temperature range. One indication is already the accurate reproduction of experimental Curie temperatures[1,35] including higher-order exchange which could not be obtained at the level of Ising, Heisenberg or Kitaev models. The magnitudes of BQ exchange can be in principle extracted from accurate hysteresis loops using phenomenological models[48,49]. Importantly in such analysis are potential temperature variations of BL and BQ exchanges with layer thickness which may indicate tunable interlayer exchanges still to be explored in 2D magnets. Frustrated 2D Heisenberg models in the presence of BQ exchange interactions are also a non-trivial
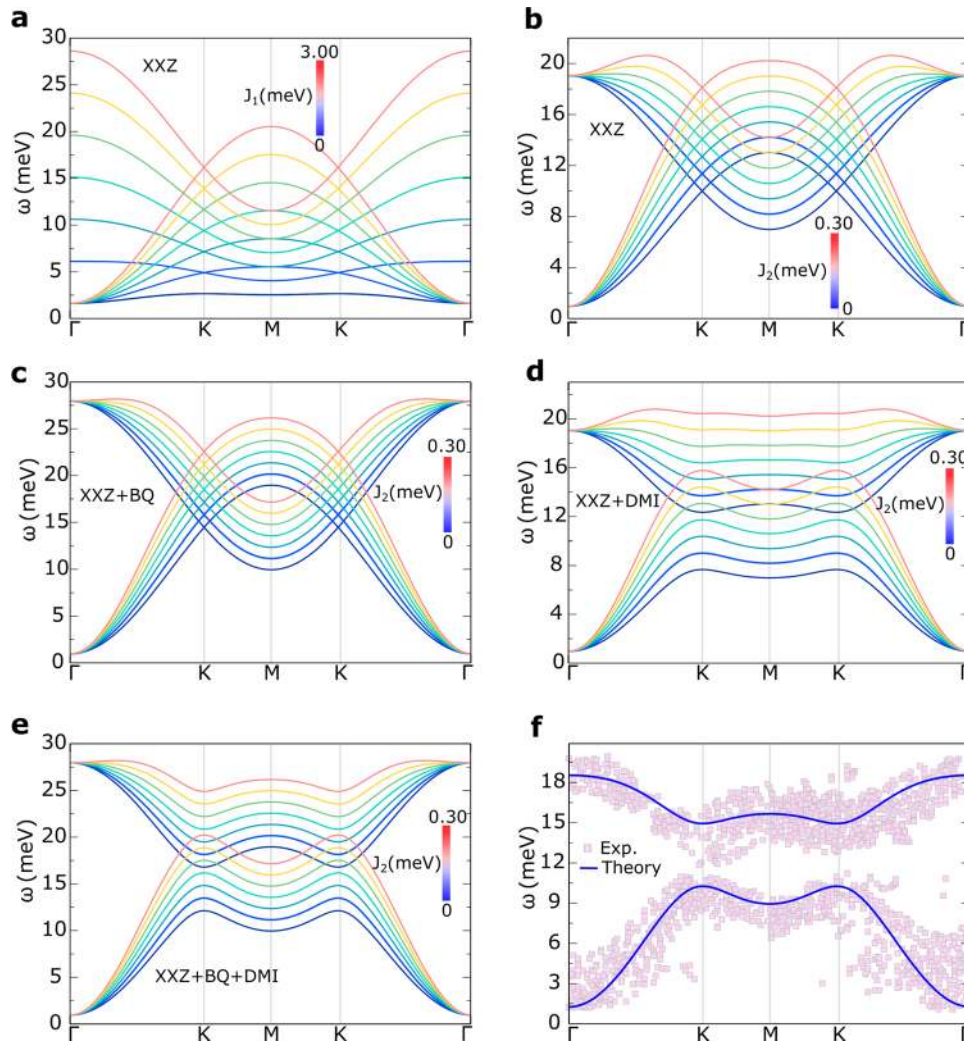
Fig. 4 Magnon spectra ω(meV) at different levels of theory for monolayer CrI₃. a ω(meV) versus **k** at the first Brillouin zone ($\Gamma - K - M - K - \Gamma$) using a XXZ model. J_1 varies within 0–3.50 meV in steps of 0.5 meV from each curve (color map). **b** Similar as a, but with a fixed $J_1 = 2.01$ meV and varying J_2 within 0–0.30 meV (color map) in steps of 0.05 meV. **c–e** ω(meV) versus **k** for different models: XXZ including BQ exchange (XXZ+BQ), XXZ including DMI (XXZ+DMI), and XXZ including both BQ exchange and DMI (XXX+BQ+DMI). In these plots, $J_1 = 2.01$ meV, $K_{bq} = 0.22$ (on **c** and **e**), $A_z = 0.31$ meV[40] (on **d** and **e**) and J_2 varies within 0–0.30 meV. **f** Comparison between the XXZ+BQ+DMI model and the experimental data[40] recently measured for bulk CrI₃. We used as parameters: $J_1 = 1.01$ meV, $J_2 = 0.10$ meV, $K_{bq} = 0.22$ meV and $A_z = 0.31$ meV[40].

matter with a rich phase diagram involving incommensurate spin spirals, canted ferromagnetic states, quadrupolar phase or vertexes[23,50–52]. As our results indicate that BQ exchanges are important for 2D magnets, possible ordered and disordered magnetic regimes may be stabilized in appreciable temperatures. Moreover, it is possible to enhance or suppress BQ interactions in Mott-Hubbard systems by applying external electric fields[53,54]. Indeed, the control of the magnetic properties of CrI₃ using electrical means has already been demonstrated[31]. Therefore, this opens the prospect of a coherent transfer between spin and charge degrees of freedom using short laser pulses in nanosheets.

METHODS
All methods can be found in Supplementary Materials.

DATA AVAILABILITY
The data that support the findings of this study are available within the paper and its Supplementary Information.

REFERENCES
1. Huang, B. et al. Layer-dependent ferromagnetism in a van der waals crystal down to the monolayer limit. *Nature* **546**, 270 –273 (2017).
2. Gong, C. et al. Discovery of intrinsic ferromagnetism in two-dimensional van der waals crystals. *Nature* **546**, 265–269 (2017).
3. Guguchia, Z. et al. Magnetism in semiconducting molybdenum dichalcogenides. *Sci. Adv* **4**, 1–8 (2018).
4. Slonczewski, J. C. Fluctuation mechanism for biquadratic exchange coupling in magnetic multilayers. *Phys. Rev. Lett.* **67**, 3172–3175 (1991).
5. Fedorova, N. S., Ederer, C., Spaldin, N. A. & Scaramucci, A. Biquadratic and ring exchange interactions in orthorhombic perovskite manganites. *Phys. Rev. B* **91**, 165122 (2015).
6. Wysocki, A. L., Belashchenko, K. D. & Antropov, V. P. Consistent model of magnetism in ferropnictides. *Nat. Phys.* **7**, 485(2011).
7. Zhu, H.-F. et al. Giant biquadratic interaction-induced magnetic anisotropy in the iron-based superconductor A_xFe$_{2-y}$Se$_2$. *Phys. Rev. B* **93**, 024511 (2016).

8. Turner, A. M., Wang, F. & Vishwanath, A. Kinetic magnetism and orbital order in iron telluride. *Phys. Rev. B* **80**, 224504 (2009).

9. Harris, E. A. & Owen, J. Biquadratic exchange between mn^{2+} ions in mgo. *Phys. Rev. Lett.* **11**, 9–10 (1963).

10. Nagaev, É. L. Anomalous magnetic structures and phase transitions in non-heisenberg magnetic materials. *Sov. Phys. Uspekhi* **25**, 31–57 (1982).

11. Gong, C. & Zhang, X. Two-dimensional magnetic crystals and emergent hetero-structure devices. *Science* **363**, 706–717 (2019).

12. Gibertini, M., Koperski, M., Morpurgo, A. F. & Novoselov, K. S. Magnetic 2d materials and heterostructures. *Nat. Nanotechnol.* **14**, 408–419 (2019).

13. Hellsvik, J. et al. Tuning order-by-disorder multiferroicity in cuo by doping. *Phys. Rev. B* **90**, 014437 (2014).

14. Novák, P., Chaplygin, I., Seifert, G., Gemming, S. & Laskowski, R. Ab-initio calculation of exchange interactions in ymno3. *Comput. Mater. Sci.* **44**, 79–81 (2008).

15. Takahashi, M. Half-filled hubbard model at low temperature. *J. Phys. C Solid State Phys.* **10**, 1289–7301 (1977).

16. Krönlein, A. et al. Magnetic ground state stabilized by three-site interactions: Fe/Rh(111). *Phys. Rev. Lett.* **120**, 207202 (2018).

17. Kurz, P., Bihlmayer, G., Hirai, K. & Blügel, S. Three-dimensional spin structure on a two-dimensional lattice: Mn/cu(111). *Phys. Rev. Lett.* **86**, 1106–1109 (2001).

18. Brinker, S., dos Santos Dias, M. & Lounis, S. The chiral biquadratic pair interaction. *N. J. Phys.* **21**, 083015 (2019).

19. Grytsiuk, S. et al. Topological–chiral magnetic interactions driven by emergent orbital magnetism. *Nat. Commun.* **11**, 511 (2020).

20. Kim, K. et al. Antiferromagnetic ordering in van der waals 2d magnetic material MnPS3 probed by raman spectroscopy. *2D Mater.* **6**, 041001 (2019).

21. Makimura, C., Sekine, T., Tanokura, Y. & Kurosawa, K. Raman scattering in the two-dimensional antiferromagnet MnPSe3. *J. Phys. Condens. Matter* **5**, 623–632 (1993).

22. Hastings, J. M., Elliott, N. & Corliss, L. M. Antiferromagnetic structures of mns$_2$, mnse$_2$, and mnte$_2$. *Phys. Rev.* **115**, 13–17 (1959).

23. Wysocki, A. L., Belashchenko, K. D. & Antropov, V. P. Consistent model of magnetism in ferropnictides. *Nat. Phys.* **7**, 485 (2011).

24. Kurz, P., Bihlmayer, G., Hirai, K. & Blügel, S. Three-dimensional spin structure on a two-dimensional lattice: Mn /cu(111). *Phys. Rev. Lett.* **86**, 1106–1109 (2001).

25. Kitaev, A. Anyons in an exactly solved model and beyond. *Ann. Phys.* **321**, 2–111 (2006).

26. Xu, C., Feng, J., Xiang, H. & Bellaiche, L. Interplay between kitaev interaction and single ion anisotropy in ferromagnetic cri 3 and crgete 3 monolayers. *npj Comput. Mater.* **4**, 57 (2018).

27. Anderson, P. W. New approach to the theory of superexchange interactions. *Phys. Rev.* **115**, 2 (1959).

28. Dionne, G. F. Magnetic Oxides (Springer, Boston, MA, 2009).

29. Mila, F. & Zhang, F.-C. On the origin of biquadratic exchange in spin 1 chains. *Eur. Phys. J.* **16**, 7–10 (2000).

30. Anderson, P. W. Theory of magnetic exchange interactions:exchange in insulators and semiconductors. (Seitz, F. & Turnbull, D. eds.). In *Solid State Physics*, vol. 14, 99–214 (Academic Press, 1963).

31. Jiang, S., Shan, J. & Mak, K. F. Electric-field switching of two-dimensional van der waals magnets. *Nat. Mater.* **1**, 406–410 (2018).

32. Evans, R. F. et al. Atomistic spin model simulations of magnetic nanomaterials. *J. Phys. Condens. Matter* **26**, 103202 (2014).

33. Ellis, M. O. A. et al. The landau–lifshitz equation in atomistic models. *Low. Temp. Phys.* **41**, 705–712 (2015).

34. Kim, H. H. et al. Evolution of interlayer and intralayer magnetism in three atomically thin chromium trihalides. *Proc. Natl Acad. Sci. USA* **116**, 11131–11136 (2019).

35. Kim, M. et al. Micromagnetometry of two-dimensional ferromagnets. *Nat. Electron.* **2**, 457–463 (2019).

36. Zhang, Z. et al. Direct photoluminescence probing of ferromagnetism in monolayer two-dimensional crbr3. *Nano Lett.* **19**, 3138–3142 (2019).

37. Mochizuki, M., Furukawa, N. & Nagaosa, N. Theory of electromagnons in the multiferroic mn perovskites: The vital role of higher harmonic components of the spiral spin order. *Phys. Rev. Lett.* **104**, 177206 (2010).

38. Dyson, F. J. General theory of spin-wave interactions. *Phys. Rev.* **102**, 1217–1230 (1956).

39. Holstein, T. & Primakoff, H. Field dependence of the intrinsic domain magnetization of a ferromagnet. *Phys. Rev.* **58**, 1098–1113 (1940).

40. Mermin, N. D. & Wagner, H. Absence of ferromagnetism or antiferromagnetism in one- or two-dimensional isotropic heisenberg models. *Phys. Rev. Lett.* **17**, 1133–1136 (1966).

41. Chen, L. et al. Topological spin excitations in honeycomb ferromagnet cri$_3$. *Phys. Rev. X* **8**, 041028 (2018).

42. Hu, J., Xu, B., Liu, W., Hao, N.-N. & Wang, Y. Unified minimum effective model of magnetic462 properties of iron-based superconductors. *Phys. Rev. B* **85**, 144403 (2012).

43. Elliott, R. J. & Thorpe, M. F. The effects of magnon-magnon interaction on the two-magnon spectra of antiferromagnets. *J. Phys. C Solid State Phys.* **2**, 1630–1643 (1969).

44. Nauciel-Bloch, M., Sarma, G. & Castets, A. Spin-one heisenberg ferromagnet in the presence of biquadratic exchange. *Phys. Rev. B* **5**, 4603–4609 (1972).

45. Coldea, R. et al. Spin waves and electronic interactions in la$_2$cuo$_4$. *Phys. Rev. Lett.* **86**, 5377–5380 (2001).

46. Haldane, F. D. M. Model for a quantum hall effect without landau levels: Condensed-matter realization of the "parity anomaly". *Phys. Rev. Lett.* **61**, 2015–2018 (1988).

47. Owerre, S. A. Topological honeycomb magnon hall effect: a calculation of thermal hall conductivity of magnetic spin excitations. *J. Appl. Phys.* **120**, 043903 (2016).

48. Basov, D. N., Averitt, R. D. & Hsieh, D. Towards properties on demand in quantum materials. *Nat. Mater.* **16**, 1077–1088 (2017).

49. Strijkers, G. J., Kohlhepp, J. T., Swagten, H. J. M. & de Jonge, W. J. M. Origin of biquadratic exchange in Fe/Si/Fe. *Phys. Rev. Lett.* **84**, 1812–1815 (2000).

50. Fullerton, E. E. & Bader, S. D. Temperature-dependent biquadratic coupling in antiferromagnetically coupled fe/fesi multilayers. *Phys. Rev. B* **53**, 5112–5115 (1996).

51. Hayden, L. X., Kaplan, T. A. & Mahanti, S. D. Frustrated classical heisenberg and *xy* models in two dimensions with nearest-neighbor biquadratic exchange: exact solution for the ground-state phase diagram. *Phys. Rev. Lett.* **105**, 047203 (2010).

52. Kaplan, T. Frustrated classical heisenberg model in one dimension with nearest-neighbor biquadratic exchange: Exact solution for the ground-state phase diagram. *Phys. Rev. B* **80**, 012407 (2009).

53. Läuchli, A., Mila, F. & Penc, K. Quadrupolar phases of the s = 1 bilinear-biquadratic heisenberg model on the triangular lattice. *Phys. Rev. Lett.* **97**, 087205 (2006).

54. Barbeau, M. M. S., Eckstein, M., Katsnelson, M. I. & Mentink, J. H. Optical control of competing exchange interactions and coherent spin-charge coupling in two-orbital Mott insulators. *SciPost Phys.* **6**, 27 (2019).

AUTHOR CONTRIBUTIONS

E.J.G.S. conceived the idea, supervised the project and undertook the analysis. A.K. performed the first-principles and Monte Carlo simulations under the supervision of E.J.G.S. R.F.L.E. implemented the biquadratic exchange interactions in the Monte Carlo algorithm. M.A., A.K. and E.J.G.S. developed the analytical and numerical models used to describe the biquadratic exchange and DMI. K.S.N. contributed on the discussions and significance of the results. E.J.G.S. wrote the paper with inputs from all authors. All authors contributed to this work, read the manuscript, discussed the results, and agreed to the contents of the manuscript.

COMPETING INTERESTS

The authors declare no conflict of interests.

ADDITIONAL INFORMATION

Supplementary information is available for this paper at https://doi.org/10.1038/s41524-020-00416-1.

Correspondence and requests for materials should be addressed to E.J.G.S.

Reprints and permission information is available at http://www.nature.com/reprints

Publisher's note Springer Nature remains neutral with regard to jurisdictional claims in published maps and institutional affiliations.